Optimization of MIM Rectifiers for Terahertz Rectennas

S.B. Tekin[a], S. Almalki[a], A. Vezzoli[b], L. O'Brien[b], S. Hall[a], P.R. Chalker[c], and I.Z. Mitrovic[a]

[a]University of Liverpool, Department of Electrical Engineering & Electronics, Brownlow Hill, Liverpool L69 3GJ, UK
[b]University of Liverpool, Department of Chemistry, Crown Street, Liverpool, L69 7ZD, UK
[c]University of Liverpool, School of Engineering, Brownlow Hill, Liverpool, L69 3GH, UK

Metal-Insulator-Metal (MIM) rectifiers comprising thin films of Al_2O_3, ZnO, NiO and Nb_2O_5 and metal configurations of Au/Au, Au/Zn and AuCr/AuCr, have been fabricated using atomic layer deposition and radio-frequency sputtering. The effect of device area scaling from 10^4 µm^2 to 1 µm^2 on rectification properties, in particular zero-bias dynamic resistance (R_0) and zero-bias responsivity (β_0) has been studied and found to be of critical importance in improving diode coupling efficiency. A significant increase of current has been found for Au/3.3 nm ZnO/Au diode when compared to the reference Au/3 nm Al_2O_3/Au diode, that resulted in obtaining the lowest R_0 of 540 Ω for a device area of 10^4 µm^2. The best performing device is found to be 1 µm^2 AuCr/6.77 nm NiO/AuCr featuring (R_0, β_0) = (461 kΩ, 0.76 A/W) and a coupling efficiency of 1.5×10^{-5} %.

Introduction

There is a significant demand for harvesting renewable infrared (IR) energy from unused heat sources. The rectifying antenna (rectenna) device has the ability to capture alternating current (AC) IR radiation and rectify it into usable direct current (DC) electricity (1). Metal-Insulator-Metal (MIM) diodes have shown to be the most prominent contenders for rectenna applications. This is due to their ultra-fast current transport mechanism in the femtosecond range by means of quantum mechanical tunnelling. Optical rectification at 28.3 THz has recently been demonstrated by rectenna devices based on MI^{n}M diodes using Au/Al_2O_3/Ti (2) and Ti/TiO_2/ZnO/Al (3) configurations. Although the results are promising, the overall conversion efficiency is low, 2.05×10^{-14} (2), mainly due to poor rectification properties of associated diodes. Other recent research (4-6) has focused on the combination of stoichiometric and non-stoichiometric oxides with the aim of engineering the barrier heights to achieve low zero-bias dynamic resistance (R_0) and high zero-bias responsivity (β_0) where the results are very promising for self-biased rectennas. The most recent experimental breakthrough was achieved with Ni/NiO/AlO_x/CrAu bowtie rectennas that feature a device area of 0.035 µm^2, R_0 of 13 kΩ and β_0 of 0.5 A/W. The results show that 5.1% coupling efficiency and 1.7×10^{-8} % power conversion efficiency can be achieved with correct optimization of the oxide stack, utilising also the effect of resonant tunnelling in lowering the dynamic resistance to match the antenna. Furthermore, the most recent theoretical study (7) shows that the β_0 of the MI^{2}M diodes can be further improved to ~ 5 A/W by keeping the impedance match between the diode and the antenna at around 100 Ω. The proposed Ti/1 nm TiO_2/1 nm Nb_2O_5/Ti rectenna design can achieve diode cut-off frequency (f_c) of 17 THz and resistance × capacitance (RC) time constant of 9 fs assuming a diode area of 0.01 µm^2. The Liverpool group has demonstrated recently (8,9) the effect of resonant tunnelling in non-cascaded (Al/Ta_2O_5/Nb_2O_5/Al_2O_3/Al) and cascaded ($Al/Nb_2O_5/Al_2O_3/Ta_2O_5/Al$) triple insulator diode structures deposited by atomic layer deposition (ALD) with an oxide thickness ratio of 1:3:1 (in nm). The diodes exhibit superior β = 5 A/W at 0.2 V and asymmetry, η = 12 at 0.1 V, with a drawback of high R_0 due to high barrier heights between the metal/oxide layers.

In this paper, we aim to further optimize the MIM diode configurations to achieve low zero-bias resistance and increase coupling efficiency with the antenna part. This is achieved by using rectenna contender oxides such as Al_2O_3, NiO, ZnO and Nb_2O_5 that have high electron affinity and low dynamic permittivity (10). Thin (≤ 7 nm) insulating layers were fabricated using radio frequency (RF) magnetron sputtering and ALD. Metal electrodes were deposited by thermal evaporation and RF sputtering using shadow mask and photolithography processes. The device areas range from 100 μm × 100 μm to 1 μm × 1 μm depending on the patterning process, to observe the effect of device scaling on the DC rectification properties. The deposited oxides were measured by variable angle spectroscopic ellipsometry (VASE) to ascertain their thickness, uniformity and optical constants. The DC current voltage (*I-V*) measurements were performed on fabricated diodes to evaluate key rectification parameters such as R_0, β_0 and η at zero-bias. Complementary theoretical calculations were performed to substantiate the experimental results and indicate that the MIM diode coupling efficiency at 28.3 THz can reach 9.75% for NiO, 14.3% for ZnO and 28.85% for Al_2O_3 based diodes of device area of 0.01 μm^2 and R_0 of 1 kΩ. The best performing experimental diode is found to be 1 μm^2 AuCr/6.77 nm NiO/AuCr featuring (R_0, β_0) = (461 kΩ, 0.76 A/W) with a coupling efficiency of 1.5×10^{-5} %.

Device Fabrication and Experimental Details

The MIM diode structures were fabricated on (i) ultra-smooth (0.32 nm rms roughness) 4 cm×4 cm Corning glass using shadow mask evaporation as shown in Fig. 1 (a), and (ii) on 300 nm SiO_2 on Si substrates using photolithography, as depicted in Fig. 1 (b). Ultra-smooth 300 nm thick SiO_2/Si substrates were used to ensure insulation and uniformity of the bottom electrode (BE) metal contacts. The process flow of the rectenna fabrication and the device cross-sections for these two different methods (shadow mask and photolithography) are shown in detail in Figs. 1(a)-(b) The proposed rectenna array consists of 1×2 rectenna elements and each element is formed by two circular patch antennas and an MIM rectifier. After the cleaning of the substrates in DECON 90 with de-ionised water (DIW), acetone, propanol and UV ozone, patterning was done and deposition of circular patch bottom antenna metal. The lift-off was performed using a conventional photolithography tool using S1813 positive photoresist and deposition equipment that included RF sputtering and evaporation. The device areas range from 10^4 μm^2 for devices processed by shadow mask, while photolithography enabled the processing of smaller devices of 64 μm^2, 16 μm^2, 4 μm^2 down to 1 μm^2 area. The device fabrication is finalised by depositing the top electrode (TE) as depicted in Fig. 1, which constitutes antenna arms. The three nominal thicknesses for oxide films were: 3 nm, 5 nm and 7 nm. The ALD of 3 nm Al_2O_3 films was done at 140 °C using trimethylaluminum (TMA) as the Al precursor and H_2O as the oxygen-containing co-reactant. The number of ALD cycles was used to control the thickness of the films. 1 TMA cycle consisted of a 20 ms TMA dose/ 2 s purge/ 20 ms H_2O dose/2 s purge. The 5 nm Al_2O_3, ZnO, Nb_2O_5 and 5-7 nm NiO films were deposited by RF sputtering using a 4-5 sccm Ar gas flow rate and a power of 45 W. Cr and Au metal electrodes were fabicated by thermal evaporation, while Zn was deposited by RF sputtering using a 5 sccm Ar gas flow rate and a power of 52.5 W. The metal electrode thickness was ~30 nm. The reference samples of deposited oxide films on n-Si(100) were fabricated simultaneously in the ALD or sputtering chamber to determine thickness and optical properties of the films using VASE. Spectroscopic ellipsometry measurements were conducted using a J.A. Woollam ellipsometer with a spectral range of 0.7-5.2 eV at 60-75˚ in 5˚ steps. Room temperature *I-V* measurements were performed in a dark probe station, using an Agilent B1500 semiconductor parameter analyzer. A summary of the fabricated MIM diode structures is shown in Table 1.

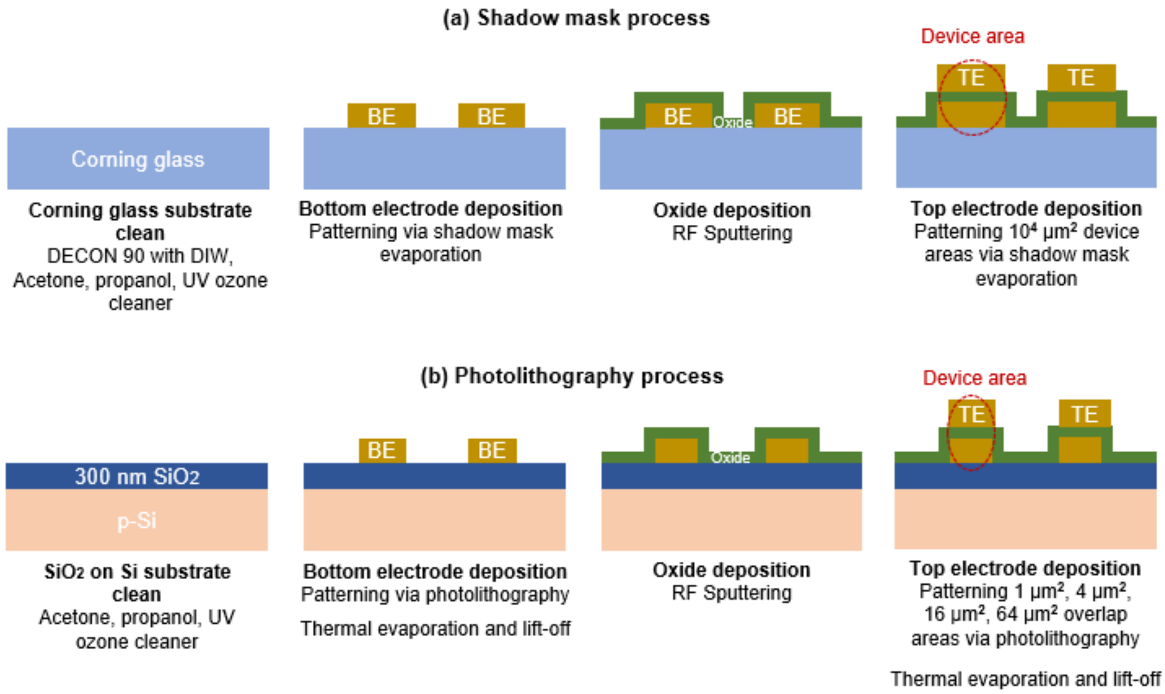

Figure 1. The fabrication process flow for patterning the layers of rectenna array at the cross-section with the integrated MIM rectifier using: (i) shadow mask; (b) photolithography process.

<u>Optical Constants of Oxide Films by VASE</u>

The thickness of four different oxides (Al_2O_3, ZnO, NiO and Nb_2O_5) studied in this paper was measured on Si reference samples by VASE in the spectral range of 240-1700 nm (0.7 – 5.2 eV). At first, the reference Si wafer was measured to ascertain the thickness of the native oxide which was then used in subsequent fittings of oxide/Si samples. Since Al_2O_3 is a transparent material, the Cauchy model was used for the VASE data fitting, whereas for ZnO, NiO and Nb_2O_5 B-Spline and general-oscillator models were used due to their UV-absorbing nature. The Kramers-Kronig consistency between the real and the imaginary part of the dielectric function was preserved in the fittings. The mean squared error (MSE) between the experimental and theoretical (fitted) (ψ, Δ) versus photon energy data curves was in all cases below 5, consistent with a good quality fit. The values of thicknesses are summarised in Table 1. It can be seen that the thiknesses are in good agreement with the nominal values, that is ±0.1 nm for ALD films and ± 0.3 nm for sputtered films. The optical constants, the refractive index (n) and the extinction coefficient (k) versus photon energy plots for Al_2O_3, ZnO, NiO and Nb_2O_5 are shown in Figs. 2(a)-(d) respectively. No absorption can be seen for Al_2O_3 up to 5.2 eV as expected since its band gap is known to be ~6.4 eV [11]. In contrast, there is a clear increase of the extinction coefficient at ~3.3 eV for ZnO (Fig. 2(b)), 3.5 eV for NiO (Fig. 2(c)) and 3.6 eV for Nb_2O_5 (Fig. 2(d)), indicating band gap values well below 5 eV. The extracted band gaps of the ZnO, NiO and Nb_2O_5 films as well as n @ 632.8 nm (1.96 eV) are consistent with the reported values in the literature (see Table 1 in Ref. 10).

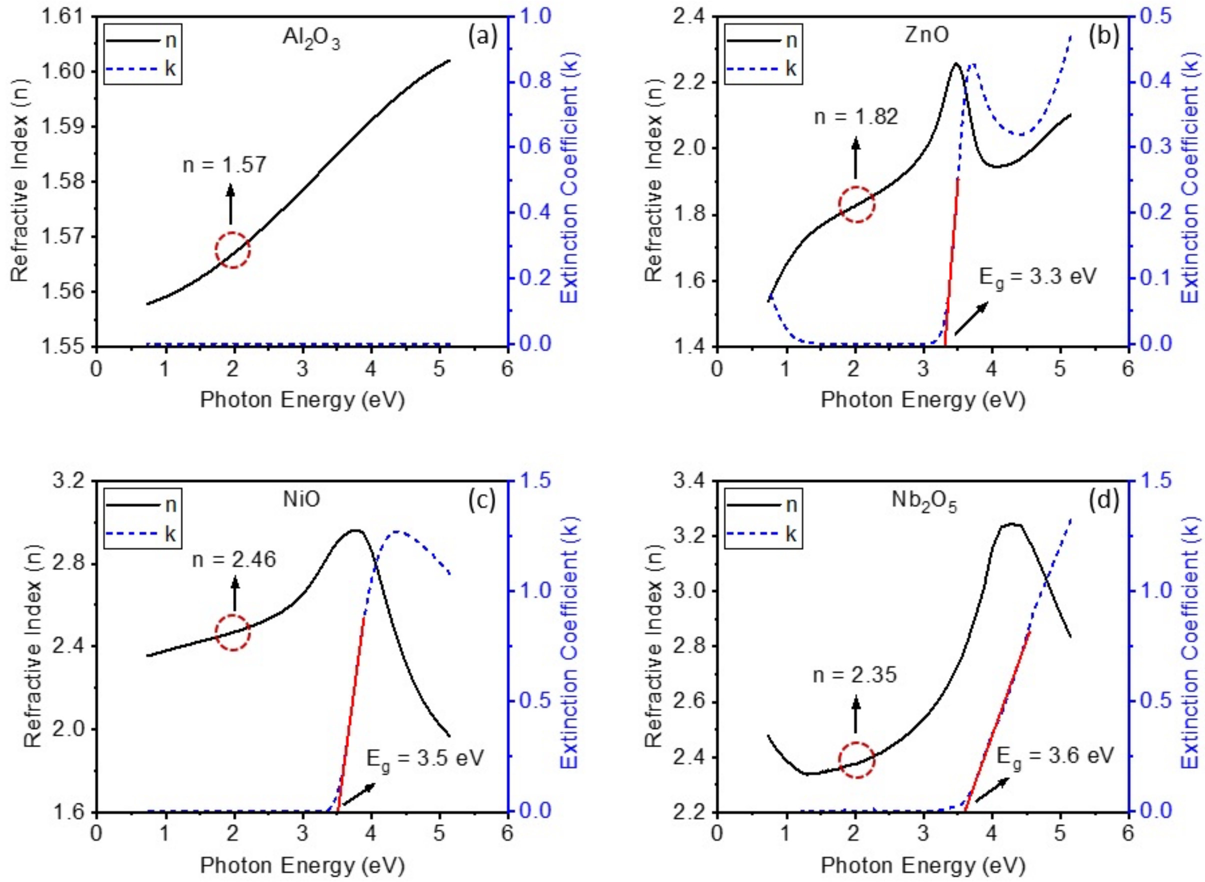

Figure 2. Refractive index (n) and extinction coefficient (k) versus photon energy plots for: (a) Al_2O_3, (b) ZnO, (c) NiO and (d) Nb_2O_5 films on Si substrates. The extraction of band gap (E_g) from linear extrapolation of the extinction coefficient edge can be seen for ZnO, NiO and Nb2O5 in (b)-(d) plots. The value of refractive index at 632.8 nm (1.96 eV) for the oxides is stated on each plot.

Rectification Behaviour of MIM Diodes with 10^4 μm^2 Device Area

The experimental *I-V* curves of three MIM devices fabricated by shadow mask evaporation are shown in Fig. 3(a) together with extracted rectification parameters of dynamic resistance ($R = (dI/dV)^{-1}$) in Fig. 3(b), responsivity ($\beta = dI''(V)/2I'(V)$) in Fig. 3(c) and asymmetry ($\eta = |I_+/I_-|$ or $|I_-/I_+|$, where I_+ refers to forward bias current and I_- to reverse bias current) in Fig. 3(d). Three types of diodes, two symmetric (with Au/Au electrodes) and one asymmetric (with Au/Zn electrodes) can be compared. The work function difference of ~0.8 eV between Au/Zn (10) influences the increased asymmetry of ~1.5 of this diode when compared with the other two with Au/Au and $\eta \sim 1$. Due to a smaller Au/ZnO barrier, there is a considerable increase of current for Au/ZnO/Au diode when compared to Au/Al_2O_3/Au, resulting in a very low zero-bias resistance of 540 Ω (Fig. 3(b)). The latter represents critical improvement to a state-of-the-art Ti/ZnO/Pt diode (12) with reported R_0 =1200 Ω and β_0 of ~0.1 comparable to β_0 of 0.06 in this work (see Table 1).

Theoretical *I-V* characteristics using the same diode structures as in Fig. 3(a) can be generated using the MATLAB in-house simulation model (13,14). The model is based on the transfer matrix method (TMM). The current density is calculated using the Tzu-Ezaki equation and subsequent transfer matrix multiplications. The dielectric layer is assumed to consist

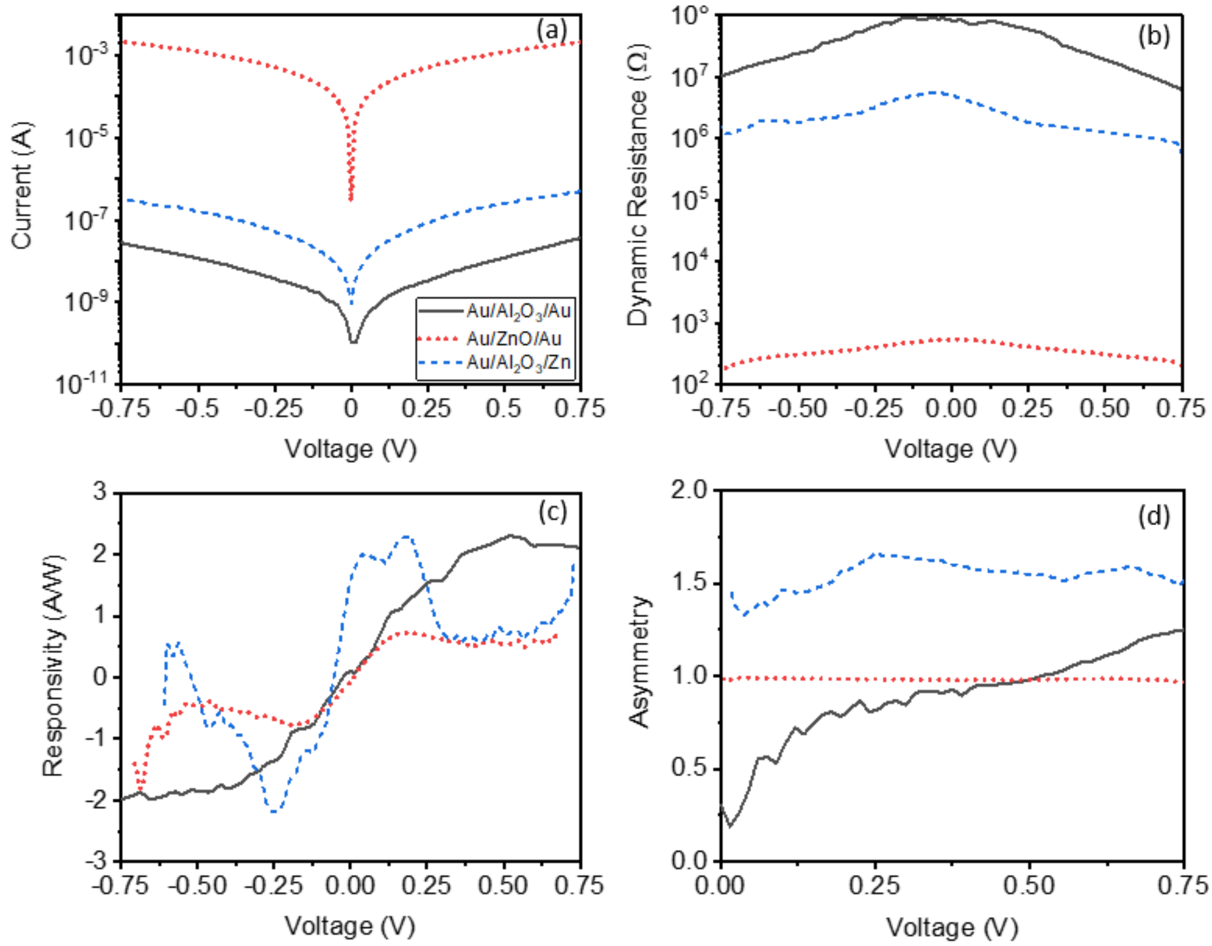

Figure 3. (a) The experimental *I-V* characteristics and associated extracted rectification parameters: (b) *R,* (c) β and (d) η for $Au/Al_2O_3/Au$, $Au/ZnO/Au$ and $Au/Al_2O_3/Zn$ diodes with nominal oxide thickness of 3 nm. The diode area is 10^4 μm^2.

of multiple slices having different barrier heights by the multi barrier Tzu-Ezaki method. Typically, 50 slices per nanometer is chosen for a sufficient simulation accuracy. The parameters used in simulations shown in Fig. 4 are (10,15): the work functions of Au and Zn are taken as 5.1 and 4.3 eV respectively, electron affinity of Al_2O_3 is 1.60 eV and of ZnO is 3.7 eV, the dielectric constant of Al_2O_3 is 10 and of ZnO is 9.4, while electron effective mass is $m_{eff} = 0.3m_0$, where m_0 is the free electron mass. A similar trend to Fig. 3(a) can be seen from the simulations shown in Fig. 4(a). As can be seen from both experimental and theoretical *I-V* curves in Figs. 3(a) and 4(a), lowering the barrier height between metal/oxide interface induces several orders of magnitude increase of current and causes a significant decrease in the device dynamic resistance (Figs. 3(b) and 4(b)). Further improvement of rectification parameters can be achieved by lowering the barrier height by using metals with lower work functions (16,17) or fabricating multiple insulator MI^nM diodes to achieve the resonant tunneling conduction mechanism (5,9,10).

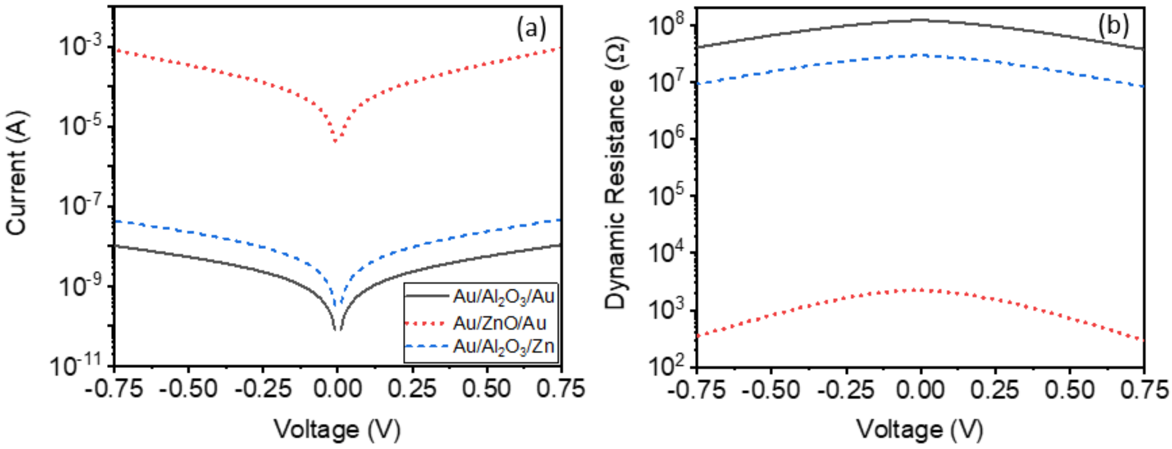

Figure 4. (a) The simulated *I-V* characteristics of diode structures shown in Fig. 3(a), with associated derived (b) dynamic resistances using in-house MATLAB model.

Effect of Device Scaling & Barrier Height on Rectification Behaviour of MIM Diodes

Figure 5 shows *I-V* characteristics and associated rectification parameters of CrAu/7 nm NiO/CrAu diodes fabricated by photolithography using four different areas, from 64 μm^2 to 1 μm^2, to investigate the effect of scaling on the device rectification. As can be seen in Figs. 5(a)-(b), reducing the device area causes decrease in the current level and an increase in the dynamic resistance as expected. The smallest R_0 was found to be 29 kΩ for the 64 μm^2 NiO-based diode, while values of 75.9 kΩ, 156.6 kΩ and 461.0 kΩ were observed for 16 μm^2, 4 μm^2 and 1 μm^2 devices respectively. There is also an increase in zero-bias responsivity (Fig. 5(c)) with decreasing device area, despite the symmetric nature of the diodes. The highest β_0 was found to be 0.76 A/W for 1 μm^2 diode being in advance to state of the art values reported to be ~ 0.5 A/W (5,16,17). The asymmetry, η (Fig. 5(d)) for all devices was found to be ~1 due to the symmetric metal electrode configurations and could be enhanced using dissimilar metals.

The effect of metal/oxide barrier height on rectification is studied using CrAu electrodes and three oxides with varying electron affinity: Al_2O_3, Nb_2O_5 and NiO. These devices have area of 64 μm^2. As shown in Fig. 6(a)-(b), the highest current level and the lowest associated R_0 was measured for the NiO diode which is about an order of magnitude higher than for Nb_2O_5 and ~5 orders of magnitude higher than Al_2O_3 based diode. This is a significant current enhancement due to the difference in metal/oxide barrier heights as reported in the literature (5,10). The β_0 values (Fig. 6(c)) for Al_2O_3, Nb_2O_5 and NiO were calculated to be 2.15 A/W, 2.10 A/W and 1.81 A/W, respectively. Since the β_0 values for these three oxides are close to each other, this makes NiO and Nb_2O_5 better contenders for the THz rectennas compared to the Al_2O_3 due to their lower R_0 values. The assymetries are also shown in Fig. 6(d), which are again close to 1 for NiO and Nb_2O_5 and the relatively higher η of Al_2O_3 can be attributed to the noise coming from experimental artifacts.

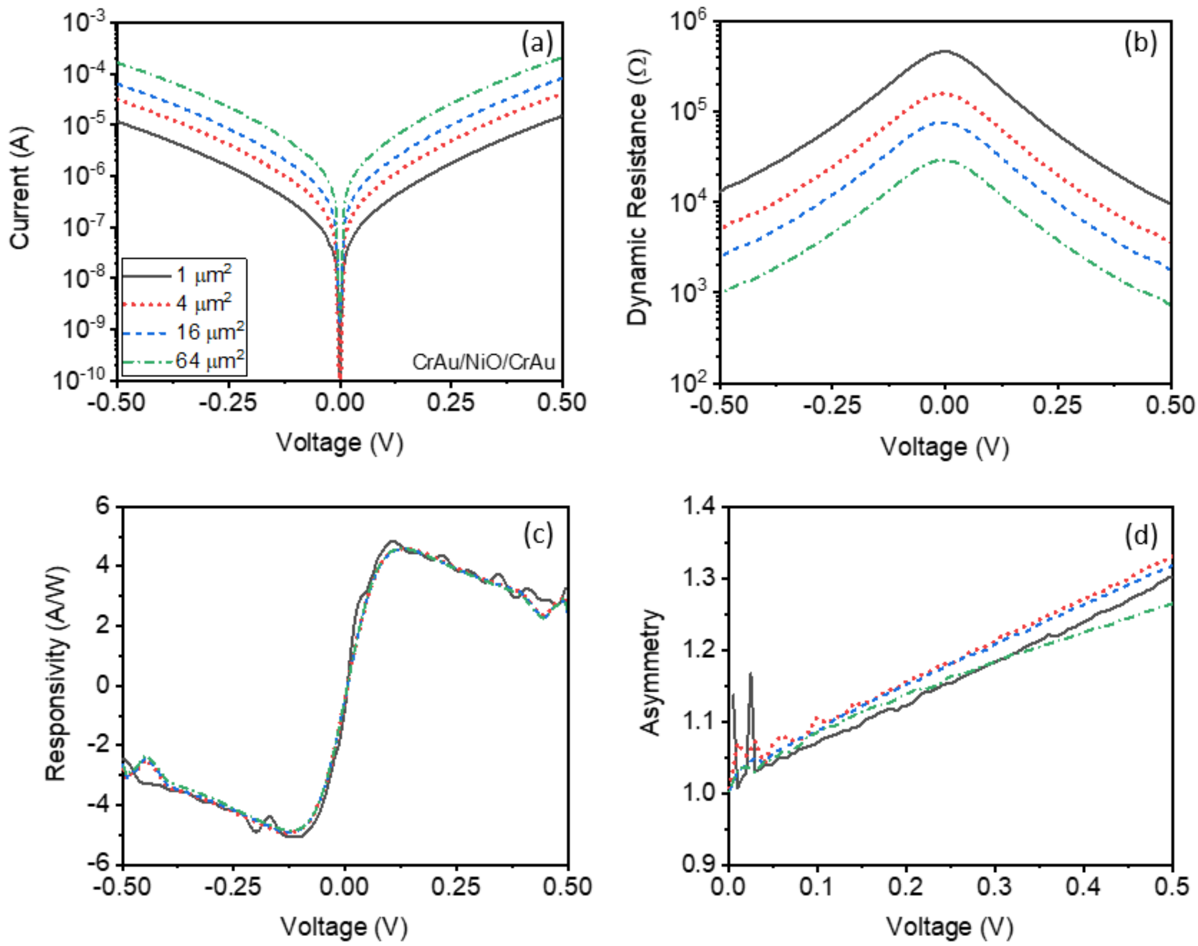

Figure 5. (a) The experimental *I-V* characteristics with associated extracted rectification parameters: (b) R, (c) β and (d) η for CrAu/NiO/CrAu diodes with varying areas, from 64 μm^2 to 1 μm^2. The nominal NiO thickness is 7 nm.

In summary, the values of rectification parameters for all MIM diode configurations in this work are shown in Table 1. It can be seen that the result of R_0 = 461 kΩ for 1 μm^2 CrAu/NiO/CrAu in this work is comparable to a diode of 1.45 μm^2 area processed by plasma oxidation that has reported value of R_0 = 500 kΩ (17). It can be seen that when the area is reduced to 0.018 μm^2, the reported R_0 for Ni/NiO/Ni diode is significantly increased to 42.4 MΩ (16) limiting its application in IR rectenna. The latest published work (5) shows that only when an extra insulator layer of AlO_x is introduced to NiO in AlO_x/NiO double insulator MIM configuration, it is possible to engineer reasonably low R_0 of 13 kΩ with the small device area of 0.035 μm^2.

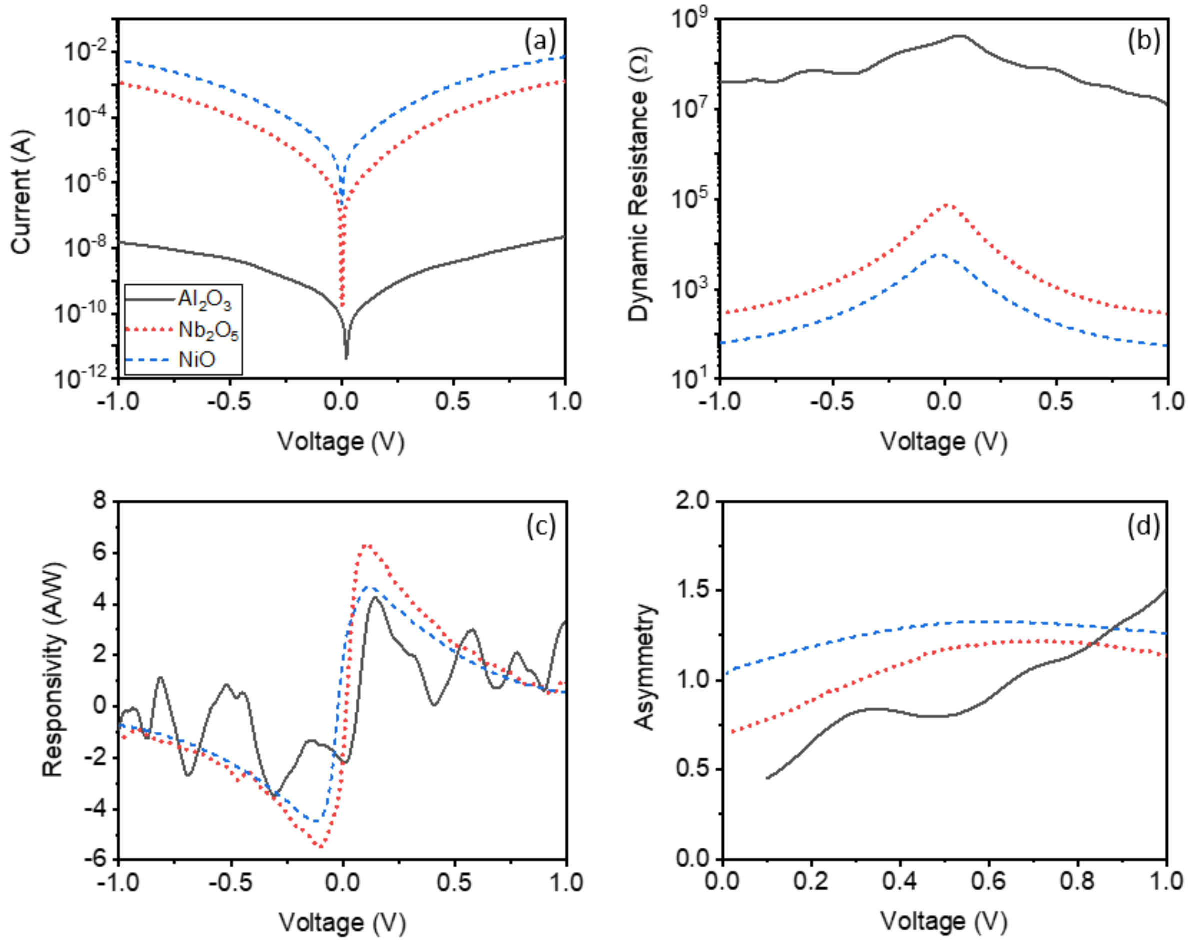

Figure 6. (a)-(d) The experimental *I-V* characteristics with associated extracted rectification parameters *R, β* and *η* for nominal 5 nm Al_2O_3, Nb_2O_5 and NiO with CrAu/CrAu electrodes.

Table 1. A summary of rectification parameters for fabricated MIM rectifiers in this work.

Diode	**Deposition method**	**Oxide thickness (nm)**	**Area (μm²)**	η_{max}	β_0 **(A/W)**	R_0 **(Ω)**
Au/Al_2O_3/Au	ALD	2.99	10^4	1.30 @ 0.75 V	0.10	83.6 M
Au/Al_2O_3/Zn	ALD	2.99	10^4	1.70 @ 0.25 V	1.60	5.1 M
CrAu/Al_2O_3/CrAu	Sputtering	5.02	64	1.50 @ 1 V	2.15	342.1 M
Au/Al_2O_3/Ti (2)	ALD	1.5	0.04†	--	0.44	98 k
Au/ZnO/Au	Sputtering	3.30	10^4	1.00 @ 0.01 V	0.06	540.0
Ti/ZnO/Pt (12)	ALD	4.0	9×10^4	--	0.125	1.2k
CrAu/Nb_2O_5/CrAu	Sputtering	5.21	64	1.21 @ 0.71 V	2.10	69.8 k
CrAu/NiO/CrAu	Sputtering	6.77	1	1.30 @ 0.5 V	0.76	461.0 k
CrAu/NiO/CrAu	Sputtering	6.77	4	1.33 @ 0.5 V	0.45	156.6 k
CrAu/NiO/CrAu	Sputtering	6.77	16	1.32 @ 0.5 V	0.42	75.9 k
CrAu/NiO/CrAu	Sputtering	6.77	64	1.26 @ 0.5 V	0.40	29.0 k
CrAu/NiO/CrAu	Sputtering	4.98	64	1.33 @ 0.56 V	1.81	5.6 k
Ni/NiO/Ni (16)	Plasma oxidation	<4.0	0.018	--	-0.41	42.4 M
Ni/NiO/CrAu (17)	Plasma oxidation	~3	1.45	--	0.5	500k
Ni/NiO/AlO_x/CrAu (5)	Sputtering	4/1	0.035	--	0.5	13k

† Device area calculated based on stated dimensions.

Discussion on Rectenna Coupling Efficiency

The energy conversion through the diode rectifier occurs by means of the resistance difference between the forward and reverse bias currents (10). Thus, the received AC signal is converted to a DC voltage. The efficiency of a rectenna can be calculated as

$$\eta = \eta_a \eta_s \eta_c \eta_j \qquad [1]$$

where η_a is the coupling efficiency of incident electromagnetic radiation to the receiving antenna, η_s is the efficiency of collected energy in the diode-antenna junction, η_c is the power coupling efficiency between the diode and antenna and η_j is the diode rectifying efficiency, which is determined by device responsivity. The power coupling efficiency (η_c) between the diode and the antenna at a specific angular frequency ω can be calculated by

$$\eta_c = \frac{4\frac{R_A R_D}{(R_A+R_D)^2}}{1+\left[\omega\frac{R_A R_D}{(R_A+R_D)}C_D\right]^2} \qquad [2]$$

where R_A and R_D are antenna and diode resistances, respectively, and C_D is the diode capacitance. The antenna reactance is assumed to be negligible compared to the diode reactance in Eq. [2] and at high frequencies (>1 THz), this effect can reduce the coupling efficiency by a factor of ≥10 (6).

If we consider the case of a full impedance match between the diode and the antenna then the antenna has a resistance of 100 Ω for capturing IR radiation. Furthermore, let us assume the same diode resistance as the antenna. Figure 7 shows the power coupling efficiency at 28.3 THz of a rectenna that includes an MIM diode from the oxides studied in this work: Al_2O_3, Nb_2O_5, ZnO and NiO. The oxide thickness was fixed at 3 nm in the calculations. The area and the dynamic resistance values were varied between 0.01 and 1 μm^2 and 100 Ω–1 kΩ, respectively. The high-frequency permittivity values of oxides ($\varepsilon_\infty = n^2$, where n is the refractive index) were used for the capacitance calculations as reported in (10,18-21): 0.8 for Al_2O_3, 2.4 for ZnO, 3.24 for NiO, all @ 28.3 THz and 22 for Nb_2O_5 at 1 THz as data for 28.3 THz is not available. It can be seen from Fig. 7 that the area is more critical than diode resistance, that is, even if the latter is engineered to be 100 Ω, the increase in area from 0.01 μm^2 to 1 μm^2 results in a significant reduction of coupling efficiency. As an example, for a NiO based diode with R_0 = 1 kΩ, the coupling efficiency reduces from about 10% to 0.01% when area is increased to 1 μm^2. The coupling efficiency from the best (R_0, β_0) experimental data from diodes in this work is also included in Fig. 7 for comparsion with theoretical prediction.

The Au/3.3 nm ZnO/Au diode has a coupling effiency of 5.6×10^{-11} %, while for CrAu/6.8 nm NiO/CrAu is 1.5×10^{-5} %. There has been a report of overall efficiency of rectenna based on Au/1.5 nm Al_2O_3/Ti diode (2) published to be 1.75×10^{-14}; based on the calculations in (2), the coupling effieciency is derived to be 1.9×10^{-3} %. The two orders of magnitude improvement in coupling efficiency is likely to be due to a smaller 1.5 nm thickness used for Al_2O_3 in comparison to thicker 6.8 nm NiO fabricated in this work. The results indicate that to achieve coupling efficiency above 10%, Al_2O_3, ZnO and NiO are all feasible providing the area can be controlled to 0.01 μm^2 while keeping the R_0 in the range of few kΩ. The latest published data summarised in Table 1 (2,5) provide further evidence that keeping the area to 0.04 μm^2 with single insulator MIM diode cannot lower R_0 sufficiently to couple IR signals, even with thicknesses of dielctric as small as ~1 nm. A combination of a double or triple insulator diode is required.

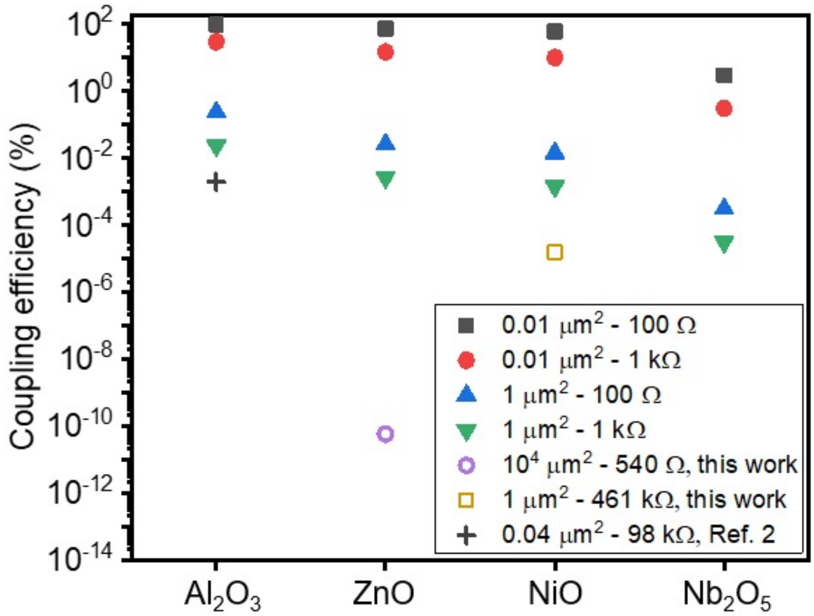

Figure 7. Calculated coupling efficiency for the MIM rectenna devices at 28.3 THz (10.6 μm) for oxides studied in this work. The experimental data for two best performing diodes, Au/3.3 nm ZnO/Au and CrAu/6.77 nm NiO/CrAu are added to the graph for comparsion.

Summary

The optimisation of rectification parameters in MIM diodes for IR rectennas has been studied in this paper, in particular focusing on reduction of zero-bias dynamic resistance by lowering the metal/oxide barrier heights. The four oxide contenders were studied: Al_2O_3, ZnO, NiO and Nb_2O_5. The effect of scaling device area down to 1 μm^2 has also been considered and found to be more critical in enhancing diode power coupling efficiency to antenna part than the reduction in R_0. A significant increase of current has been found for Au/3.3 nm ZnO/Au diode when compared to the reference Au/3 nm Al_2O_3/Au diode, that resulted in obtaining the lowest R_0 of 540 Ω for device area of 10^4 μm^2. The best performing device is found to be 1 μm^2 AuCr/6.77 nm NiO/AuCr featuring (R_0, β_0) = (461 kΩ, 0.76 A/W) and a coupling efficiency of 1.5×10^{-5} %. Further scaling to 0.01 μm^2 device size area is necessary to achieve coupling efficiency above 10%, while keeping the dynamic resistance low (~ kΩ) with ultra-thin stack in double or triple insulator MI^{n}M configuration. This study clearly demonstrates the potential of several oxides in MIM rectifiers for operation at THz frequencies.

Acknowledgement

The authors thank EPSRC, UK, project number EP/K018930/1 and British Council UGC-UKIERI project numbers IND/CONT/G/17-18/18 and F.No.184-1/2018(IC) for funding the work.

References

1. S. Hall, I. Z. Mitrovic, N. Sedghi, C. S. Yao-chun, Y. Huang, J. F. Ralph, *Funct. Nanomater. Devices Electron. Sensors Energy Harvest*. 241–265 (2014).
2. G. Jayaswal, A. Belkadi, A. Meredov, B. Pelz, G. Moddel, and A. Shamim, *Mater. Today Energy*, **7**, 1–9 (2018).
3. A. Y. Elsharabasy, A. S. Negm, M. H. Bakr, and M. Jamal Deen, *IEEE J. Photovoltaics*, **9**, 1232–1239 (2019).
4. D. Matsuura, M. Shimizu, and H. Yugami, *Sci. Rep.* **9**, 1–7 (2019).
5. A. Weerakkody, A. Belkadi, and G. Moddel, *ACS Appl. Nano Mater*. **4**, 2470–2475 (2021).
6. A. Belkadi, A. Weerakkody, and G. Moddel, *Nat. Commun*. **12**, 1–6 (2021).
7. A. Y. Elsharabasy, M. H. Bakr, and M. J. Deen, *Results Mater*.,**11**, 100204 (2021).
8. I. Z. Mitrovic, A. D. Weerakkody, N. Sedghi, S. Hall, J. F. Ralph, J. S. Wrench, P. R. Chalker, Z. Luo, S. Beeby, *ECS Trans*. **72**, 287 (2016).
9. S. B. Tekin, A. D. Weerakkody, N. Sedghi, S. Hall, M. Werner, J. S. Wrench, P. R. Chalker, I. Z. Mitrovic, *Solid State Electron*., **185**, 108096 (2021).
10. I. Z. Mitrovic, S. Almalki, S. B. Tekin, N. Sedghi, P. R. Chalker, and S. Hall, *Materials*, **14**, 5218 (2021).
11. I. Z. Mitrovic, M. Althobaiti, A. D. Weerakkody, V. R. Dhanak, W. M. Linhart, T. D. Veal, N. Sedghi, S. Hall, P. R. Chalker, D. Tsoutsou, A. Dimoulas, *J. Appl. Phys*. **115**, 114102 (2014).
12. A. A. Khan, G. Jayaswal, F.A. Gahaffar, A. Shamim, *Microelectron. Eng*. **181**, 34–42 (2017).
13. N. Sedghi, J. F. Ralph, I. Z. Mitrovic, P. R. Chalker, and S. Hall, *Appl. Phys. Lett*., **102**, 092103 (2013).
14. N. Sedghi, J. W. Zhang, J. F. Ralph, Y. Huang, I. Z. Mitrovic, and S. Hall, *In Proceedings of the 2013 European Solid-State Device Research Conference (ESSDERC)*, 131–134 (2013).
15. B. Hussain, A. Aslam, T. M. Khan, M. Creighton, and B. Zohuri, *Electronics,* **8**, 238 (2019).
16. K. Choi, F. Yesilkoy, G. Ryu, S. H. Cho, N. Goldsman, M. Dagenais, M. Peckerar, *IEEE Trans. Electron Devices*, **58**, 3519–3528 (2011).
17. S. Krishnan, H. La Rosa, E. Stefanakos, S. Bhansali, K. Buckle, *Sens. Actuators A Phys*. **142**, 40–47 (2008).
18. Z. Thacker and P. J. Pinhero, *IEEE Trans. Terahertz Sci. Technol*. **6**, 414–419 (2016).
19. K. Z. Rajab et al., *J. Microelectron. Electron. Packag*., **5**, 2–7 (2008).
20. Y. Kim, M. Yi, B. G. Kim, and J. Ahn, *Appl. Opt*., **50**, 2906–2910 (2011).
21. N. Matsumoto, T. Hosokura, K. Kageyama, H. Takagi, Y. Sakabe, and M. Hangyo, *Jpn. J. Appl. Phys*., **47**, 7725–7728 (2008).